# Seismic Response of Partial-Joint-Penetration Welded Column Splices in Moment-Resisting Frames

SEAN M. SHAW, KIMBERLY STILLMAKER and AMIT M. KANVINDE


## ABSTRACT

Current standards require that welded column splice connections in special or intermediate moment-resisting frames (SMRFs or IMRFs) feature complete-joint-penetration (CJP) groove welds to develop the full flexural strength of the column. In contrast to partial-joint-penetration (PJP) welds, CJP welds are often costly, requiring additional material, inspection and back-gouging or backing-bar removal to ensure complete penetration. However, unlike welded beam-column connections, which fractured in the 1994 Northridge Earthquake, column splices have modest deformation demands. This suggests that perhaps with modern, toughness-rated weld filler materials and welding practice, PJP welded splices may offer acceptable performance under seismic loads. Motivated by these observations, a study featuring five full-scale tests on PJP-welded column splices is presented to examine their feasibility for use in IMRFs or SMRFs in seismic environments. The test matrix investigates a range of parameters, including column sizes (consistent with use in 4-, 9- and 20-story buildings) as well as variations in connection details (single and double-beveled, welded and unwelded webs, presence of a weld access hole). All specimens utilized columns with specified yield strength 50 ksi for the columns and ultimate strength 70 ksi for the weld electrode. The specimens were loaded cyclically in a three-point bend configuration such that the splice was subjected to demands consistent with those in severe earthquakes; a loading protocol was developed specifically for this purpose based on nonlinear time history simulations. All the full-scale specimens exhibited excellent performance, such that the splices exceeded the moment capacity of the smaller connected column. The full-scale data is complemented by a series of ancillary tests such that the results may be interpreted with respect to measured, rather than specified, material properties. A series of finite element fracture mechanics simulations is also presented to assist with the generalization of test results. The finite element simulations indicate that for the tested connections, the toughness demands are below the minimum expected toughness, suggesting that details similar to the ones tested in the study may be suitable for general use in the field. A synthesis of the test and simulation data is encouraging from the perspective of adoption of PJP welded splices in IMRFs and SMRFs in seismic regions. Limitations of the research are outlined, along with discussion of future work to develop further support for the use of PJP welded splices in moment frames.



**Keywords:** partial-joint-penetration groove welds, PJP welds, column splices, moment frames.


## INTRODUCTION

The 1994 Northridge earthquake revealed the susceptibility of welded beam-to-column (WBC) connections to fracture. Numerous studies associated with the SAC Steel Project (SAC, 1996), such as Engelhardt and Sabol (1994), exhaustively examined the factors responsible for these fractures and developed recommendations for new construction as well as retrofit (FEMA, 2000). By and large, these studies concur that the WBC fractures may be attributed to a combination of low toughness in the base and/or weld material; poor detailing practice, such as the use of backing bars and weld runoff tabs, which produced flaws or cracks in highly stressed regions of the flanges; and connection configurations that did not account for unanticipated stress distributions, such as the amplification of shear and longitudinal stress in the flanges due to inadequate participation of the web connection. Informed by these investigations, subsequent design standards such as the 2010 AISC *Seismic Provisions for Structural Steel Buildings* (AISC 341-10) mandate stringent requirements for material toughness [based on Charpy V-notch (CVN) testing of base and weld material], detailing, and guidelines for connection design and inspection. As a result, the fracture risk in WBC connections has been mitigated to a large extent.

The post-Northridge research discussed previously primarily addressed WBC connections because a vast majority of the fractures during the Northridge earthquake were observed in these connections. However, the broader findings regarding the fracture-susceptibility of details with effect of sharp flaws and brittle materials resulted in updated design requirements for other connections as well. These include column splice connections, which are commonly used in moment frames due to one or more of the following reasons: column sections are typically transitioned to account for changes in loading over the height of the building; the


Sean M. Shaw, Design Engineer, Buehler and Buehler Structural Engineers, Sacramento, CA. Email: sshaw@bbse.com

Kimberly Stillmaker, Graduate Research Assistant, Department of Civil and Environmental Engineering, University of California, Davis, CA. Email: kstillmaker@ucdavis.edu

Amit M. Kanvinde, Associate Professor, Department of Civil and Environmental Engineering, University of California, Davis, CA (corresponding). Email: kanvinde@ucdavis.edu

height of the building is greater than the length of the available section; or shipping constraints and erection practices limit the length of the columns. To reflect the need for more stringent detailing requirements in these connections, AISC 341-10 prescribes the following for intermediate and special moment-resisting frames (IMRFs and SMRFs): "Where welds are used to make the splice, they shall be complete-joint-penetration groove welds."

Figure 1a schematically illustrates a pre-Northridge column splice connection, and Figure 1b indicates a post-Northridge connection designed using the improved guidelines outlined previously. The main difference between the pre- and post-Northridge type connections is that the post-Northridge connections incorporate complete-joint-penetration (CJP) welds in the flanges and the webs (to develop the flexural strength of the column by eliminating the crack-like flaw at the unfused weld root, UWR), whereas the pre-Northridge connections used partial-joint-penetration (PJP) welds, with weld penetration (or effective throat) in the range of 40 to 60% of the flange thickness. The newer splice details with the CJP welds are significantly more expensive to construct for several reasons. First, more weld material must be used because full penetration is required; the volume of weld material is nonlinearly proportional to the extent of penetration. Second, the use of additional weld material requires a greater number of weld passes, requiring surface preparation and cleaning between each pass. Third, and perhaps most important, complete penetration typically requires back-gouging and welding the material near the weld root from the opposite side, such that no part of the connection remains unfused. Alternative processes, such as using a backing-bar are possible as well, although sometimes undesirable due to stability concerns. Finally, demand critical CJP welds require rigorous inspection protocols. It is especially inconvenient and costly to conduct these processes because the splices are always field-welded, often several stories above the ground.

In light of these observations, it is also relevant to reference other aspects of the post-Northridge connections as well as recent research on other welded connections. Specifically, AISC 341-10 identifies the welds in the splices as demand critical welds, requiring that the weld filler metals must meet minimum toughness requirements (minimum CVN energy of 20 ft-lb at 0 °F and additionally, a CVN energy of 40 ft-lb at 70 °F from heat input envelope testing). This is significantly higher as compared to the weld materials used in pre-Northridge connections. For comparison, the E70T-4 weld filler metal typically used in pre-Northridge details exhibited CVN energy values in the range of 5 to 10 ft-lb at 20 °F (Kaufmann and Fisher, 1995). Moreover, AISC 341-10 also requires the column splice to be located either 4 ft away from the floor or at the center of the column if the story height is less than 8 ft. It is considered unlikely that this location (and hence the splice) will be subjected to high inelastic rotation demands, for the following reasons. First, the strong-column-weak-beam (SCWB) requirement encourages the development of plastic hinges in the beams, under first mode response. Second, the absence of transverse load on the column implies that the peak moments are attained at the ends (rather than in the center) of the columns; in fact, under first-mode response that dominates most low-to-mid-rise buildings, the bending moment near the center of the column approaches zero as the column bends in double curvature. Prior analytical research by Shen et al. (2010) indicates that the splices are not subjected to significant inelastic action, even under extreme seismic events. The findings of this research are confirmed by similar simulations conducted as part of the current study (described in a subsequent section of this paper). Finally, recent research on other types of connections by the lead investigator of this study, e.g., Myers et al. (2009), Gomez et al. (2010) and Dubina and Stratan (2002), indicates that when high-toughness materials (similar to those required by post-Northridge design standards) are used, the presence of

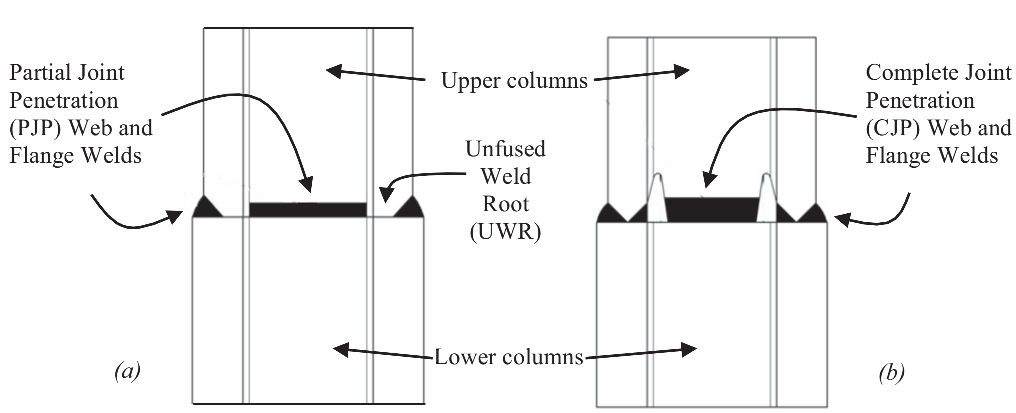


*Fig. 1. Column splice construction practice (a) pre-Northridge and (b) post-Northridge. Erection plates on web not shown for clarity.*

a flaw or crack-like stress raiser (produced, e.g., due to the UWR) may be tolerated without brittle fracture.

When considered together, the previous observations suggest that inelastic deformation demands in splices may be relatively modest and, even if these demands are present, the use of appropriately designed PJP details may successfully mitigate fracture risk. This is important, considering the expense and inconvenience of constructing CJP welds in column splices. Motivated by these observations, this paper presents a series of full-scale tests on column splice connections welded with PJP welds and high-toughness weld filler metals. The main objective of the study is to investigate the seismic performance of these connections and to examine their feasibility for use in SMRF/IMRF structures in highly seismic environments. The paper begins with a discussion of relevant literature in the area, with the objective of establishing context for the current study. This is followed by a discussion of a series of nonlinear time history simulations that were conducted to characterize the demands in column splices and to develop a loading protocol for the full-scale testing. The column splice tests (which feature Grade 50 base materials and E70 weld electrodes) are then presented, along with analysis and discussion, which also leverages ancillary tests conducted to establish material constitutive and toughness properties. The paper concludes with a discussion of fracture mechanics analysis, which examines the potential for generalization of test results.

## LITERATURE REVIEW AND OBJECTIVES

Although guidelines for the design of column splice connections are stringent and similar to other connections such as WBC connections, research directly addressing column splice connections for seismic conditions has been relatively sparse. In fact, the only experimental study on fracture-critical welded column splices was conducted by Bruneau and Mahin (1991) prior to the Northridge earthquake. Other previous studies on column splices (Popov and Stephen, 1976; and Hayes, 1957) have examined the response of spliced columns in compression. The Bruneau and Mahin study featured two column splice specimens, which connected heavy rolled sections (W14×665 connected to W14×500 and W14×426 connected to W14×370), with flanges in the thickness range of 2.6 to 4.5 in. The specimens were constructed to replicate construction practice prevalent at the time in terms of material properties, weld and member sizes, and residual stresses as well as detailing practice and welding procedures. Of these two specimens, one featured PJP welds in the flanges with 50% penetration, whereas the other featured CJP welds with weld access holes. The specimens were subjected to cyclic loading under a four-point bend configuration, such that the splice region was subjected to pure flexure. As a consequence, the effect of shear was not considered. The prominent findings of this study were that the CJP welded splice exhibited excellent performance sustaining moments greater than the cross-sectional strength of the smaller connected column, and although the PJP welded splice failed in a brittle manner, it did so after the net-section strength of the connection (the strength based on the cross-sectional area, discounting the unfused root region) was reached. This implies that locally, the weld material had sufficient toughness to allow yielding over the entire weld ligament (the connected portion), even if the corresponding strength was not sufficient to prevent brittle fracture of the connection when considered at the component scale.

The latter is an important observation in the context of the present study because weld and base materials used in the Bruneau and Mahin (1991) tests were not subject to minimum toughness requirements, which were enforced after the Northridge earthquake and ensuing research. As outlined in the introduction, toughness of contemporaneously used weld filler metals (such as E70T-4) is significantly lower than what is currently required. Thus, the performance of PJP connections in the Bruneau and Mahin study indicate the possibility of successfully using toughness rated filler materials with PJP weld details.

Nuttayasakul (2000) conducted fracture mechanics based finite element simulations of the Bruneau and Mahin (1991) tests, as well as additional parametric simulations of column splice details with PJP welds. The finite element study confirmed the internal stress distributions determined by Bruneau and Mahin. The fracture mechanics simulations also suggest that despite the absence of a minimum specified toughness, pre-Northridge weld materials may have had sufficient toughness to develop the net-section strength (at the weaker base metal) of the PJP connection, if an adequate degree of effective throat thickness (approximately 70% of the flange thickness, assuming an overmatched weld) were provided.

Shen et al. (2010) conducted a series of nonlinear time history simulations to examine seismic demands in column splices. Given the absence of similar studies prior to this, the primary aim of the Shen et al. investigation was to develop understanding of the force and deformation demands in column splices such that the margin of safety provided by current design/detailing practice could be evaluated, with a possibility of lowering the stringency of detailing requirements. The nonlinear time history simulations were conducted for 4-, 9- and 20-story moment frame buildings subjected to a suite of 20 ground motions representative of the Southern California region. The simulations revealed that even under extreme ground motions (consistent with MCE or maximum considered earthquake levels), the inelastic deformation demand in the splices is negligible, when interpreted at the macro-scale (or cross-sectional level). However, the force demands approach the capacity of the smaller connected column. Shen et al. (2010) characterized the force demands in terms of a *P-M* interaction ratio, *IR*, which reflects the combined effect of the axial tension and bending moment, such that an IR of 1.0 implies tensile yielding at the flange of the smaller (upper) connected column. This is because owing to the UWR, splice fracture is sensitive to a peak tensile stress in the flange of the connection. Consequently, the *IR* is an appropriate indicator of splice distress. As expected, the demands were highest (with a peak *IR* approximately equal to 1.0) for the 20-story building because of higher overturning moments, increasing the axial tension in the exterior columns and the pronounced participation of higher dynamic modes, resulting in single-curvature bending of some columns. The latter effect was dominant. For the 4- and 9-story frames, the force demands were significantly lower—peak *IR*, computed over all the motions for the 4-story frame was in the range 0.35 to 0.8, whereas for the 9-story frame it was in the range of 0.5 to 0.9.

A synthesis of these three studies on column splices, along with other research (e.g., Myers et al., 2009) that focused on the deformation capacity of other PJP welded connections (such as column base plates), yields the following observations:

1. The testing by Bruneau and Mahin (1991) and complementary finite element simulations by Nuttayasakul (2000) suggest that even without the enforcement of current toughness requirements, pre-Northridge type PJP welds offered sufficient toughness to develop the net-section strength of the welded flanges, provided sufficient weld penetration was provided.
2. While column splices may be subjected to high force demands (approaching the capacity of the smaller connected column), the inelastic deformation demands are minimal or absent.
3. Other types of connections that incorporate PJP welds (base plate connections featuring notch-tough material compliant with the AISC *Seismic Provisions*), tested by Myers et al. (2009) and more recently Gomez et al. (2010), show excellent performance with the capacity to fully develop the column flanges in yielding.

Based on these observations, the specific objectives of the study presented in this paper are:

1. To experimentally examine the performance of various PJP-welded column splices under a test protocol representative of seismic loading.
2. To conduct a program of ancillary material tests and fracture mechanics analysis to examine the feasibility of these connections in steel moment frame construction in seismic regions.

The next section describes the nonlinear time history simulations conducted for assessment of demands in the splices and the loading protocol developed from these simulations.

## NONLINEAR TIME HISTORY SIMULATION, DEMAND CHARACTERIZATION AND DEVELOPMENT OF LOADING PROTOCOL

An understanding of seismic demands in column splices in moment frames is critical for two reasons. First, it provides context for evaluating the vulnerability of splices that may be constructed using PJP welds. Second, and perhaps more important to this study, an analysis of the demands enables the development of a loading protocol for application to the full-scale splice specimens described in the next section. The development of such a protocol is necessary, because existing protocols for SMRF components (Gupta and Krawinkler, 1999) address seismic demands only in deformation-controlled components (such as beam-to-column connections). Column splices in SMRFs are primarily load-controlled, because inelastic deformations are not expected at the component level, albeit local yielding in the weld region is possible. Protocols for these types of components (specifically splices) are not available, nor is it appropriate to adapt protocols developed for deformation-controlled components. Consequently, the large-scale testing requires the development of loading histories that represent seismic demands at the splice in a reasonable, yet conservative manner. A comprehensive program of nonlinear time history simulations was conducted, with the specific objective of assessing splice demands in the context of developing a loading protocol. The simulations conducted in this study are targeted specifically toward the development of loading protocols. It is relevant to discuss here that previous nonlinear time history simulations targeted toward the development of loading protocols (e.g., Gupta and Krawinkler, 1999) have employed ground motions that are scaled such that they represent a target probability of exceedance, such as 10% in 50 years (also expressed as a 10/50 hazard). Figure 2 indicates the buildings used for the nonlinear time history simulations used in this study, whereas subsequent discussion addresses the nonlinear time history simulation and protocol development.

1. Three generic frames (4-, 9- and 20-story) were used—see Figure 2. These are identical to the frames used by Shen et al. (2010) and are adapted from the SAC model buildings (Gupta and Krawinkler, 1999), with the exception that the 3-story SAC model building was replaced by a 4-story building to accommodate the splice (which is uncommon for shorter buildings). The frames have fundamental periods of 0.93, 1.75 and 2.33 s, respectively. The frames were assumed to be constructed for a seismic environment

(and typical gravity loading) consistent with the Los Angeles, California, region assuming firm soil conditions (NEHRP site class D). Refer to Shaw (2013) for more details regarding the building designs. Figure 2 shows the frames, including the locations of the splices (located 4 ft from the top surface of the beam in the lower story).

2. Each frame was subjected to a suite of 20 ground motions. These motions, developed during the SAC steel project (Somerville et al., 1997) are titled LA21-LA40, and are based on recordings from the 1994 Northridge, 1995 Kobe, 1989 Loma Prieta and the 1974 Tabas earthquakes, in addition to simulated motions. The ground motions were scaled to match two spectra, consistent with the 10/50 and 2/50 hazard (per ASCE 7-10) at a general location in the Los Angeles basin. Thus, a total of 40 motions (20 × 2 scaling levels) were used.

3. The simulations were conducted on the platform OpenSEES (2009), which has the capability to simulate several physical aspects of response. The specific modeling considerations included:

   - The use of fiber sections for simulation of the beams and columns to represent axial-moment interaction and the spread of plasticity. The fiber sections utilized a bilinear steel material model with kinematic hardening. Material parameters were calibrated to match a comprehensive data set of plastic hinge response compiled previously by Lignos et al. (2011). The calibrated values of the parameters are $E$ = 29,000 ksi, $F_y$ = 55 ksi (to account for material overstrength with respect to specified strength) and the post-yield (hardening) slope of 1.7% of the initial elastic modulus.
   - Finite joint sizes were modeled. This is especially important because flexural demands at the splice are sensitive to its distance from the end of the column (at the beam face).
   - Geometric nonlinearity effects ($P$–δ and $P$–Δ) were modeled.

Several variables were monitored during the nonlinear time history simulations. While the interstory drift and inelastic rotations are of interest, the time histories of longitudinal stress at the locations of the splices (specifically in the flange regions) are determined to be the most critical in the context of this study. This is because the primary concern with respect to the PJP welded splices is fracture at the UWR (see Figure 1). This type of fracture may be considered stress-controlled, because the inelastic deformation (at the splice component level) is modest or negligible. Because both bending and axial force (due to overturning effects) contribute to the longitudinal stress, each flange within each splice is subjected to a different stress history. Recognizing this, the time history of the longitudinal stresses at the extreme fiber of the splices (in the smaller connected column) was monitored for each flange within each splice,

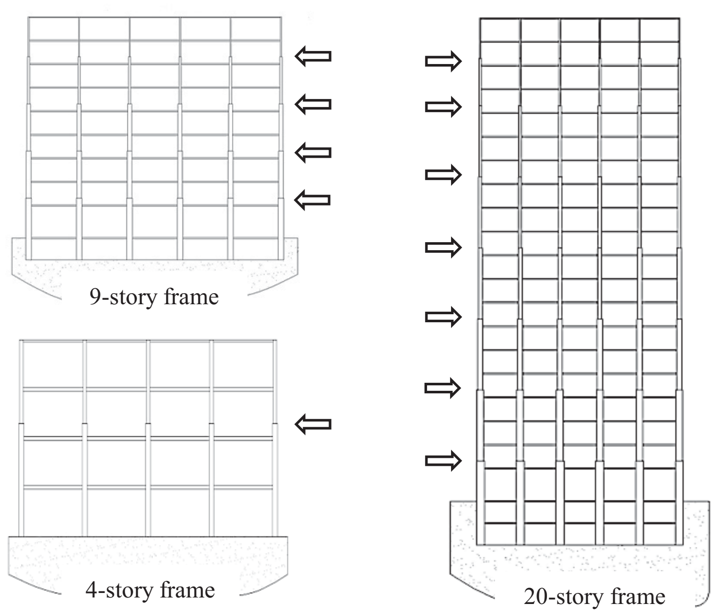


*Fig. 2. Schematic illustration of the three model buildings with arrows indicating spliced stories.*

| Table 1. Summary of Results from Nonlinear Time History Simulations | | | | | | | | |
|---|---|---|---|---|---|---|---|---|
| | Ground motions scaled to 10/50 hazard | | | | Ground motions scaled to 2/50 hazard | | | |
| Frame | $IR_{peak}^{median}$ | $IR_{peak}^{max}$ | $\Delta_{peak}^{median}$ | $\Delta_{peak}^{max}$ | $IR_{peak}^{median}$ | $IR_{peak}^{max}$ | $\Delta_{peak}^{median}$ | $\Delta_{peak}^{max}$ |
| 4-story | 0.16 | 0.30 (3E)[a] | 1.1% | 2.9% (2)[b] | 0.30 | 0.54 (3E) | 2.4% | 6.1% (2) |
| 9-story | 0.11 | 0.30 (2E) | 0.8% | 1.6% (3) | 0.23 | 0.72 (2I) | 2.0% | 5.4% (4) |
| 20-story | 0.18 | 0.72 (5E) | 0.6% | 1.5% (16) | 0.22 | 0.95 (5E) | 1.1% | 2.5% (2) |

[a] Value in parentheses indicates location of occurrence of $IR_{peak}^{max}$; (3E) indicates third-story exterior column, while (2I) indicates the second-story interior column.

[b] Value in parentheses indicates location of occurrence of $\Delta_{peak}^{max}$; (4) indicates fourth story.

for each of the nonlinear time history runs. The interaction ratio, $IR$, is a convenient indicator of the stress in the flange, normalized by the yield strength of the flange material, such that $IR = 1.0$ implies tension yielding at the extreme fiber of the cross-section. Table 1 provides an overview of the results of the nonlinear time history simulations for the three frames.

The table includes the maximum value and the median value of $IR_{peak}$ determined from 20 nonlinear time history simulations (for each of the scaling levels). The $IR_{peak}$ value presented in the table reflects the combination of axial force and moment that produces the peak tensile stress in any of the splice flanges. The corresponding flange is considered the critical flange for that nonlinear time history run. Corresponding statistics are also presented for the peak interstory drift, $\Delta_{peak}$ (observed in any of the stories within a nonlinear time history run). Referring to the table, the following observations may be made regarding frame and splice response:

1. For the 4-story frame, the interaction ratios are fairly modest. For example, $IR_{peak}^{max}$ for the 10/50 and 2/50 motions are 0.30 and 0.54, respectively. This suggests that for low-rise frames, the tensile stress in the flanges is well below the yield stress. This is consistent with intuition because the response of the 4-story frame is dominated by the first mode resulting in points of inflection near the center of the columns; thereby lowering the moment at the splice and the effects of overturning moment and the associated axial tension are modest as well.

2. For the 9-story frame, the $IR_{peak}^{max}$ are 0.30 and 0.72 for the 10/50 and 2/50 motions, respectively. These are somewhat larger as compared to the corresponding values for the 4-story frames, presumably because both the effects described previously—mode of deformation as well as overturning moments—are more prominent. However, even these are significantly lower as compared to the capacity of the smaller connected column.

3. The splices in the 20-story frame are subjected to demands that are by far the most severe. For this frame, $IR_{peak}^{max}$ for the 10/50 and 2/50 are 0.72 and 0.95, respectively, indicating that demands approach the capacity of the smaller connected column (for the 2/50 hazard), due to a combination of higher-mode response, overturning effects and the larger dynamic forces.

Referring to Table 1, for all the frames, the interstory drift ratios are in the anticipated range. While the peak tensile stress (implied by $IR_{peak}$ is an important parameter with respect to splice fracture, it is not appropriate to entirely disregard history effects in the development of the loading protocol, because the material at the tip the of UWR is also subject to local inelastic cyclic strain. To address this, a rigorous approach was adopted following the methodology originally developed for moment frame connections by Gupta and Krawinkler (1999), subsequently adapted by Richards and Uang (2006) and more recently Fell et al. (2009) for other components. Figure 3 schematically illustrates the loading protocol developed during this study for application to splice specimens. A detailed description of protocol development is provided in Shaw (2013), whereas the main features are briefly summarized as follows:

1. The primary objective of the loading protocol is to subject the PJP welds in the splice tests to stresses (including stress peaks and stress histories) that represent conservative as well as realistic demands consistent with specific seismic hazards.

2. The protocol is constructed in terms of the ratio $M_{splice} \big/ M_p^{smaller-section}$, where $M_{splice}$ is the applied (or demand) moment and $M_p^{smaller-section}$ is the plastic moment capacity about the major axis of the smaller column section, including the effect of material overstrength, taken as $M_p^{smaller-section} = R_y F_y Z_x$. Although the stresses in the splices (in archetype frames and in the nonlinear time history simulations) are a result of axial force and moments, the test apparatus (discussed in the next section) can apply only bending loads. The

loading protocol was developed such that the longitudinal stresses in the flange generated in the bending-only configuration are consistent with those implied by the nonlinear time history simulations, which are a combination of axial and bending stresses.

3. Careful consideration was given to stress-history effects. For this purpose, the following steps were carried out:
   - Each stress history was converted into equivalent constant amplitude cycles using the rainflow counting method (Matsuishi and Endo, 1968).
   - Based on these equivalent cycles, a statistical analysis of the important history parameters (e.g., the peak interaction ratio, the number of damaging cycles and cumulative stress amplitudes) was conducted with respect to the response data from the different ground motions.
   - At this point, the protocol was heuristically constructed to match or exceed specific statistical indicators (percentile values) of these history parameters. As discussed previously, Shaw (2013) provides a detailed description of these history parameters, the rationale underlying their selection, and their use in the development of the protocol.
4. Referring to Figure 3, the loading protocol indicates several checkpoints marked by text on the loading history. For example, one of the points is identified as $9_{max}$. The implication is that at this instant in the protocol, all the history indicators (indicative of damage) have been exceeded with a 100% probability in the critical flange of the 9-story frame, for all ground motions scaled to the 2/50 hazard. The primed values on Figure 3 indicate that similar demands have been met or exceeded in the other flange of the specimen (the one that is subjected to tension during the first excursion). Note that this is more conservative than the benchmark established by Gupta and Krawinkler (1999) for qualification for welded-beam-to-column connections (which utilized 86 percentile values from the 10/50 motions). The implication of this is that if a test specimen survives a particular checkpoint on the protocol, it suggests that the connection is a candidate for qualification under demands implied by that checkpoint. By extension, survival through the entire protocol suggests that the splice detail may withstand demands consistent with those in 4-, 9- and 20- story buildings.

The next section describes the full-scale testing on column splices based on this protocol, along with a summary of ancillary material testing.

## SPLICE COMPONENT TESTS

This section provides a detailed overview of the splice component tests, including the test setup, instrumentation, specimen fabrication, and finally, the test results. Table 2 includes

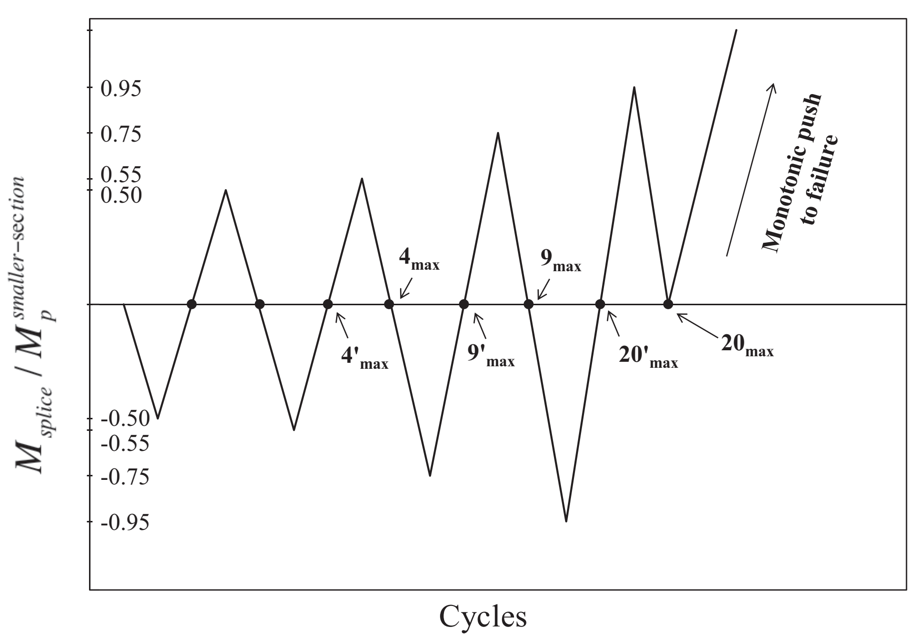


*Fig. 3. Loading protocol.*

| Table 2. Test Matrix and Summary of Key Results | | | | | | | |
|---|---|---|---|---|---|---|---|
| | Specimen Details | | | Results[a] | | | |
| **Test** | **Column Sizes** | **Weld Pen** | **Remarks[b]** | $\frac{M_{splice}^{max}}{M_p^{smaller-section}}$ | $\frac{V_{splice}^{max}}{V_y^{smaller-section}}$ | $\frac{\sigma_{flange}^{max}}{F_y^{flange}}$ | $\frac{\delta_{midspan}}{\delta_y}$ |
| **24A** | W24×370<br>W24×279 | 82% F[c]<br>87% W | Single external bevel, no access hole | 1.13 | 0.85 | 1.31 | 4.8 |
| **24B** | W24×370<br>W24×279 | 82% F<br>87% W | Single external bevel, no access hole | 1.19 | 0.89 | 1.33 | 5.8 |
| **14A** | W14×730<br>W14×550 | 82% F<br>87% W | Double beveled with access hole | 1.37 | 0.93 | 1.34 | 16.1 |
| **14B** | W14×455<br>W14×342 | 55% + 40% F[d]<br>84% W | Double beveled with no access hole, internal flange weld terminated short of web fillet | 1.24 | 0.86 | 1.34 | 5.0 |
| **14C** | W14×145<br>W14×132 | 89% F<br>0% W | Single external bevel, no access hole, bolted web plate | 1.04 | 0.72 | 1.43 | 2.0 |

[a] All referenced material properties are measured (see Table 3), rather than specified.
[b] All details are shown schematically in Figure 5.
[c] Flange and web welds denoted with F and W, respectively.
[d] 55% External flange weld, with 40% Internal flange weld terminated short of web fillet (see Figure 5c).

the test matrix summarizing key features of the five tests that were conducted. Also included in Table 2 are some of the test results, discussed later. The column sizes used in these experiments are consistent with those commonly used in design practice. For example, specimen 14A features one of the heaviest available W-sections (W14×730 connected to a W14×550). The tests may therefore be considered full-scale.

## Specimen Construction Process

Because the performance of the PJP splices is sensitive to the execution of the weld details, it is especially important that the welds in the test specimens are representative of field welds. To ensure this, specimen fabrication and erection, including weld procedures, closely followed the processes and practices consistent with field implementation. The following process was implemented:

1. Steel column sections were procured from an AISC certified fabricator and erector. Mill certificates summarizing material yield, ultimate, and toughness properties were provided along with these sections. Data from these mill certificates is provided in Table 3.
2. The sections were shipped to a fabricator where the connection details were prepared; this included surface preparation for the weld bevels and the fabrication of erection plates.
3. The site-ready subassemblies were shipped to a steel erector where column sections were welded in a vertical position in an effort to minimize variance from field conditions.
4. These types of groove welds are not currently allowed in seismic force resisting systems. As a result, a new welding procedure specification (WPS) was created for these welds. While details of the WPS are available in Shaw (2013), the main parameters of the WPS were:
    - FCAW-S welding with E70T-6 electrode (Lincoln NR-305); 3⁄32-in. diameter.
    - Deposit rate (travel speed) was 12-10 in./min.
    - Minimum preheat temperature 350 °F (this is conservatively in excess of the 225 °F minimum required by AWS D1.1-2004 due to the welding of jumbo sections); interpass temperature between 350 and 500 °F.
    - Current: 430–470 A; Voltage: 25–26 V.
5. A procedure qualification record (PQR) was created to support the welding procedure. Data from the PQR testing (on a mockup assembly constructed to represent the splice welds) is provided in Table 3, along with similar data for the base metals (obtained from the mill certificates).

| Table 3. Material Tensile and Toughness Data from Ancillary Testing | | | | | | | | |
|---|---|---|---|---|---|---|---|---|
| Material source ↓ | | $F_y$[a] (ksi) | $F_u$[a] (ksi) | $F_y/F_u$[a] | Elongation[a] (%) | CVN[a] at 0 °F ft-lb | CVN[a] at 70 °F ft-lb | CVN[a] at 70 °F ft-lb |
| Applicable requirement[b] → | | 50-65 ksi | ≥65 ksi | ≤0.85 | ≥21% | ≥20 ft-lb | | ≥20 ft-lb |
| **Base metal Test 24A** | W24×370 | 55.1 | 70.3 | 0.78 | 34 | Not applicable | | 149 |
| | W24×279 | 56.8 | 71.7 | 0.79 | 39 | | | 200 |
| **Base metal Test 24B** | W24×370 | 54.5 | 70.2 | 0.78 | 38 | | | 149 |
| | W24×279 | 56.9 | 71.9 | 0.79 | 33 | | | 200 |
| **Base metal Test 14A** | W14×730 | 56.2 | 71.0 | 0.79 | 34 | | | 292 |
| | W14×550 | 53.8 | 70.5 | 0.76 | 38 | | | 227 |
| **Base metal Test 14B** | W14×455 | 57.0 | 73.9 | 0.77 | 36 | | | 297 |
| | W14×342 | 52.8 | 71.3 | 0.74 | 28 | | | 104 |
| **Base metal Test 14C** | W14×145 | 75.4[4] | 87.2 | 0.86[c] | 21 | | | Not applicable[d] |
| | W14×132 | 54.2 | 77.7 | 0.70 | 31 | | | |
| **Weld** | **PQR** | All-weld coupons were not tested for tensile properties, only toughness tests were conducted | | | | 52 | Not tested | Not applicable |
| | **W14B post test** | | | | | Not tested | 50 | |

[a] Average data from three coupon tests.
[b] Based on AISC 341-10.
[c] Does not meet applicable standard.
[d] Base material toughness requirements are only applicable to heavy sections, both W14×145 and W14×132 are not categorized as heavy as per the 14th edition Steel Construction Manual (AISC, 2011).

6. Upon completion, all the welds were inspected visually and with ultrasonic testing by independent inspectors. During this process, a crack was discovered at the root pass of specimen 14C. The deficient weld was removed and re-welded. Subsequent inspection of the repaired weld revealed no cracks.

These construction processes are common to all specimens; specific weld details are discussed in the subsection on experimental response.

## Ancillary Testing for Characterization of Material Toughness and Constitutive Properties

The large scale tests were complemented by a comprehensive program of ancillary tests, summarized in Table 3. Table 3 also summarizes the permissible values for each quantity measured in the ancillary tests. The program comprised the following types of tests.

### *Tension Tests*

A total of 30 coupons (three replicates from the smaller column and larger column section of each of the five large-scale test specimens) were tested to establish yield and ultimate properties for the base materials. Referring to Table 3, the yield, ultimate and elongation properties are mostly within the permissible range, with the exception of the material for W14×145 that exhibited strengths higher than the maximum allowable. However, the W14×145 is the larger column within specimen 14C, whereas the test protocol and benchmark performance is expressed in terms of the strength of the smaller column.

### *Charpy V-Notch Tests*

Tests were conducted on coupons extracted from the base as well as weld material. For the base material (heavy sections), AISC 341-10 requires a minimum CVN toughness of 20 ft-lb at 70 °F for specimens extracted from the core of the cross section. For demand-critical welds, the minimum requirement is 20 ft-lb at 0 °F. In addition, a value of 40 ft-lb at 70 °F from heat input envelope testing is also required for the weld filler metal (to qualify the electrode). To support the weld procedure specifications for the current testing program, and to provide insight into the response of the fabricated connections, the following supplementary data was obtained:

- *CVN coupons from the PQR weld assembly.* This involved the testing of CVN coupons at 0 °F to demonstrate that the joint could meet AISC 341-10 by exhibiting a CVN energy of 20 ft-lb at this temperature. Referring to Table 3, a value of 52 ft-lb (well in excess of 20 ft-lb) was obtained.

- *CVN coupons from the compression flange of specimen 14B*. Additional CVN coupons were extracted from the compression (unfractured) flange of one of the full-scale test specimens after the completion of the test; these were tested at 70 °F. The toughness data from these tests does not reflect the intent of AISC 341-10 given that the compression flange is subjected to several inelastic cycles before the CVN extraction and testing. However, these tests provide an indication of the toughness of the as-deposited weld at room (or test) temperature. The average CVN value (from 3 coupons) was 50 ft-lb.

In addition to establishing compliance with applicable standards, the ancillary tests serve both to enable the interpretation of full-scale data with respect to measured, rather than specified material properties, and to enable the calibration of material constitutive and fracture toughness properties in finite element simulations (discussed in a subsequent section).

**Test Setup and Instrumentation**

Figure 4 schematically illustrates the test setup used for testing. Several factors controlled the design of the setup, including limitations in the size, configuration and capacity of the testing machine as well as the necessity to provide loading and boundary conditions that reflected field conditions with realism.

The specimens were all tested as beams in three-point bending, with a load applied at midspan. The splice is located at a distance of 18 in. from midspan, such that it is subjected to a combination of flexure and shear.

The testing machine applies load only in the downward direction. Cyclic loading was applied by rotating or flipping the specimen about its longitudinal axis after every loading excursion implied by the loading protocol shown previously in Figure 3. Although the loading apparatus cannot apply axial tension, the loading protocol is developed such that flange stresses are consistent with those produced due to a combination of axial tension and bending in building columns.

All specimens were loaded in an identical manner: cyclic loading was applied at midspan as per the loading protocol, until either failure was observed or the machine capacity was exceeded (the latter happened only in the case of specimen 14A). Note that the values in the loading protocol are the moments at the splice location normalized by the expected strength ($M_p^{smaller-section} = R_y F_y Z_x$) of the specimen; these

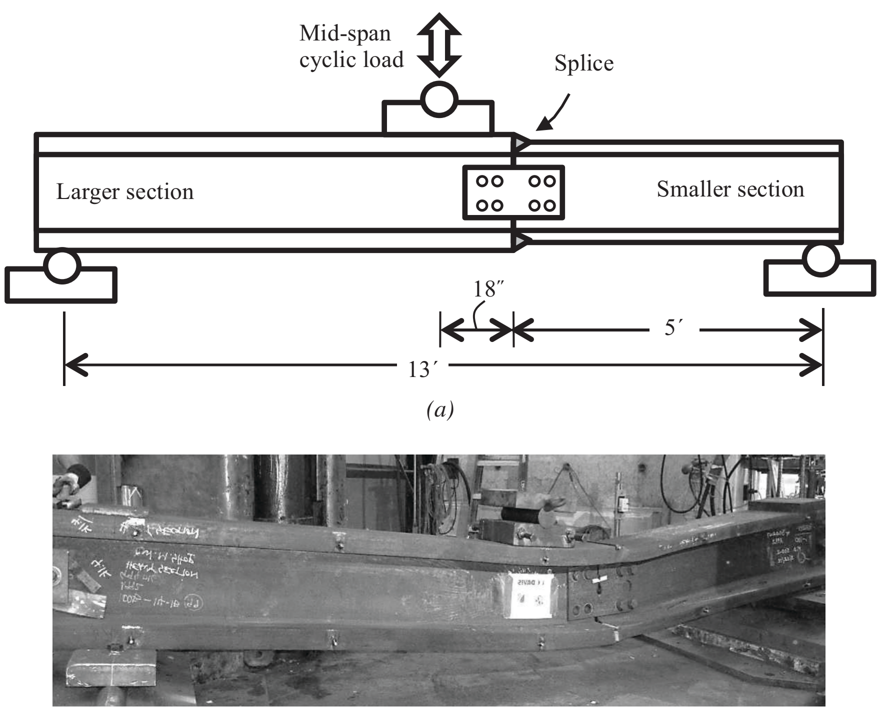


*Fig. 4. (a) Schematic illustration of test setup, and (b) specimen 14B overview after test.*

were converted to an equivalent midspan load for testing. The specimens were extensively instrumented. The primary control variable was the midspan force, and the associated splice moment. The midspan and splice deflections were also monitored. Strain gages were placed at multiple locations, including the flanges of the splices and the webs. The purpose of the web strain gages (rosettes) was to examine the distribution of shear between the web and the flanges. These are especially relevant for the bolted web connection (specimen 14C), in which the load path for the shear force is not as rigid as for the other (welded web) specimens. Secondary instrumentation was installed to monitor unanticipated response such as out-of-plane buckling. However, this type of response was not observed for any of the tests. The instrumentation was complemented by still and video cameras. Being supported by the Network for Earthquake Engineering Simulation (NEES), all the data from the project is freely available for download from the NEES data repository.

### Test Matrix

Referring to the test matrix shown previously in Table 2, five specimens were tested. The main consideration in the selection of the section sizes was realism, such that these sections are of a comparable scale to those typically specified in moment frames. Testing archetype-scale components is especially important in the context of weld fracture because scale-effects in fracture (Bažant, 1984; Anderson, 1995) are well known, wherein fracture mechanics must be invoked, often with some subjectivity, to generalize test results. Also, the thermo-mechanical process of heat-transfer, cooling and phase change that occur during welding affect weld toughness and may be scale dependent, especially if multi-pass welds are used. Finally, the residual stress patterns in large specimens are likely to be different than those developed in small-scale specimens due to the constraint to shrinkage provided by the larger sections. All details were designed in consultation with the steel fabricator and erector, as well as AISC, to provide an efficient means of obtaining the desired level of weld penetration representative of future practice (if, based on this study, PJP welds are determined to be suitable for column splices). Highlights of the test matrix are as follows (refer to Table 2):

1. **Tests 24A and 24B.** Two replicate specimens featuring W24 columns (specifically W24×279 attached to W24×370) were tested. The size of these sections is representative of usage in 15- to 20-story moment frame buildings. Figure 5a schematically illustrates the splice detail for these specimens. The flanges (2.09 in. for the W24×279 and 2.72 in. for the W24×370) were connected with one PJP weld on the outside of the flange, equivalent to 82% penetration with respect to the smaller (W24×279) flange. Because only an external weld with a single bevel was used, a weld access hole was not provided in the web. The web featured a single beveled PJP weld with 87% with respect to the thinner (W24×279) web. A bolted erection plate, sized for erection loads, was provided as also indicated in Figure 5a.
2. **Test 14A.** This specimen was fabricated from a W14×730 column connected to a W14×550; which are two of the heaviest available W-sections. In fact, the flange sizes are 4.91 and 3.82 in. for the larger and smaller columns, respectively, requiring the largest possible weld in a column splice for W-sections. Figure 5b schematically illustrates the splice detail for this specimen. The flanges were double beveled and welds were provided on the inside and outside of the flanges. The total connected penetration was 82% with respect to the smaller (W14×550) flange. A weld access hole (in compliance with AWS D1.8, 2009) was provided in the web. The web featured a single-sided PJP weld with 87% penetration. Similar to the W24 specimens, a bolted erection plate was provided. This plate was ground to follow the contour of the weld access hole.
3. **Test 14B.** This specimen was fabricated from a W14×455 column connected to a W14×342, which have flange sizes 3.21 and 2.47 in. for the larger and smaller columns, respectively. Referring to Figure 5c, the flange of the smaller column was double beveled, similar to specimen 14A. The external weld penetration was 55%, whereas the internal weld penetration was 40% (with respect to the thinner flange). However, the internal bevel (and weld) was stopped short of the web fillet. Thus, the detail was designed to examine the performance of a cost-effective connection that did not require a weld-access hole. From a fracture mechanics perspective, this absence of the continuous weld on the inside of the flange generates a large unfused area in the k-region of the columns. An erection plate was provided, similar to the W24 specimens.
4. **Test 14C.** This specimen features the smallest specimens, a W14×145 connected to a W14×132. These member sizes are representative of those typically used in low-to-mid-rise frames (roughly 2 to 5 stories tall), which constitute a large percentage of the building stock. The flange of the smaller column was provided with a single, external bevel and a PJP weld with 89% penetration. No weld access hole was provided. The distinguishing characteristic of this specimen was that the webs of the columns were not welded; rather, a bolted web-splice plate was provided for shear transfer

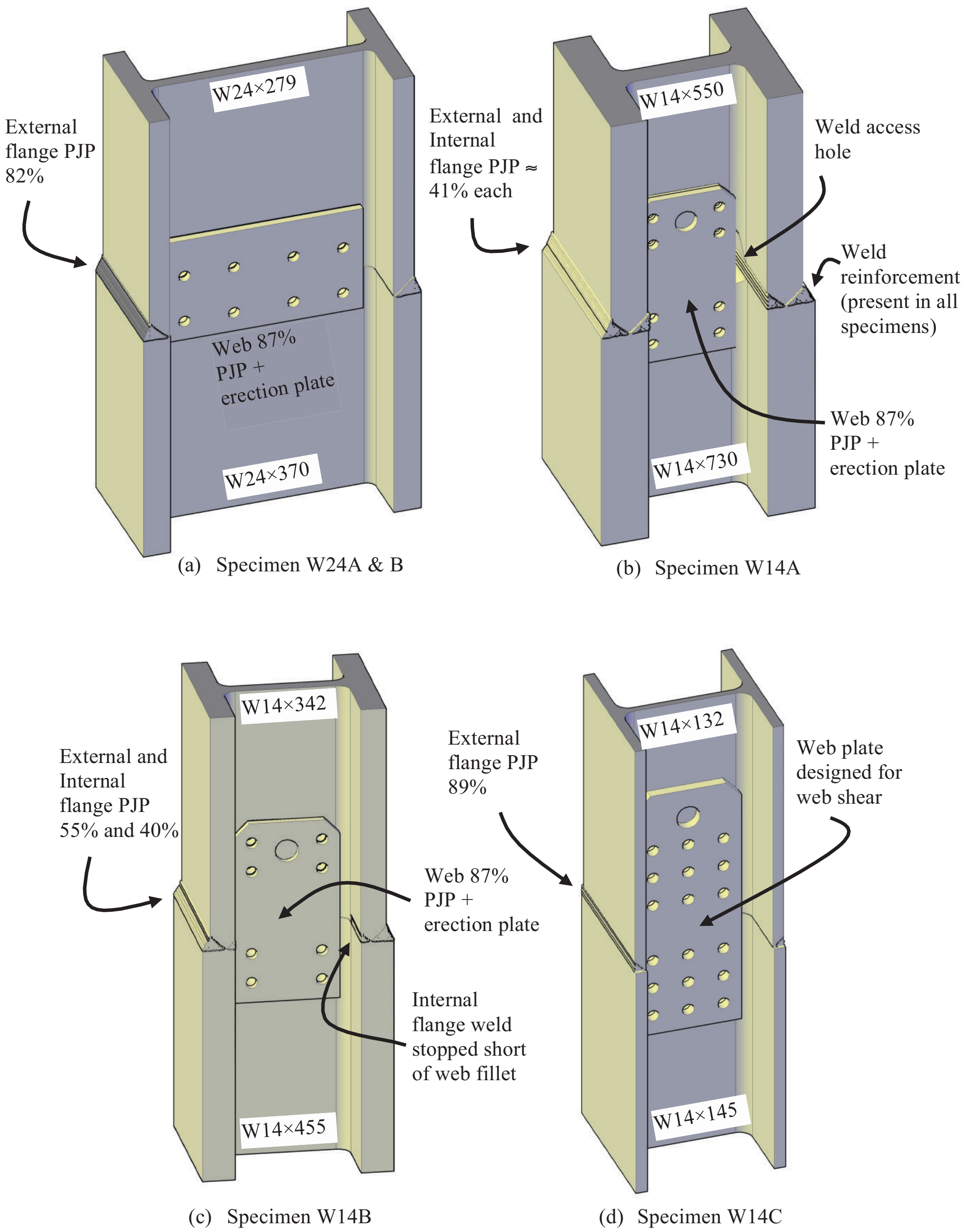


*Fig. 5. Splice connection details.*

between the webs. Post-Northridge research (FEMA, 2000) indicated that bolted webs are inefficient in transferring shear, producing secondary bending in the flanges and increasing the susceptibility to premature fracture. However, referring to previous discussion, Table 1, and the loading protocol shown in Figure 3, recall that the force demands for low-to-mid-rise frames are rather modest, with $IR_{peak}^{max} < 0.5$. With this consideration, specimen 14C was designed in this manner to explore the possibility of an economical connection for low-to-mid-rise frames. The web plate was designed to develop the full shear capacity of the web, and the bolt pattern was determined assuming an eccentrically loaded bolted connection (Shaw, 2013). Figure 5d illustrates this detail schematically.

For all the specimens, a smooth transition was obtained between the thicker and the thinner flange (indicated on Figure 5a, but representative of all the specimens), in compliance with AWS D1.8 (2009). This has two implications. First, the flared shape of the weld provides reinforcement at the section of the UWR. Second, no sharp discontinuities or re-entrant corners, other than the UWR itself, are present in the detail. The next section describes the qualitative and quantitative results from the splice experiments.

## Experimental Observations

Table 2 summarizes results from all the tests. All the specimens survived the cyclic portion of the loading history (shown in Figure 3), and all (with the exception of specimen 14A, which did not fail because machine capacity was reached) failed during the final monotonic push. This implies that all specimens exhibited excellent performance when assessed in the context of demands imposed by the loading protocol. Figures 6a through 6d illustrate the load-deformation response of all the splice connections. The loads indicated on Figure 6 are expressed in terms of the moment at the splice (normalized by the plastic moment, based on measured material properties) versus the midspan deflection. The primary indicators of performance are the peak moment at the splice—this was always observed during the final cycle; the estimated stress in the flange at the splice; and the peak shear at the splice. These quantities are

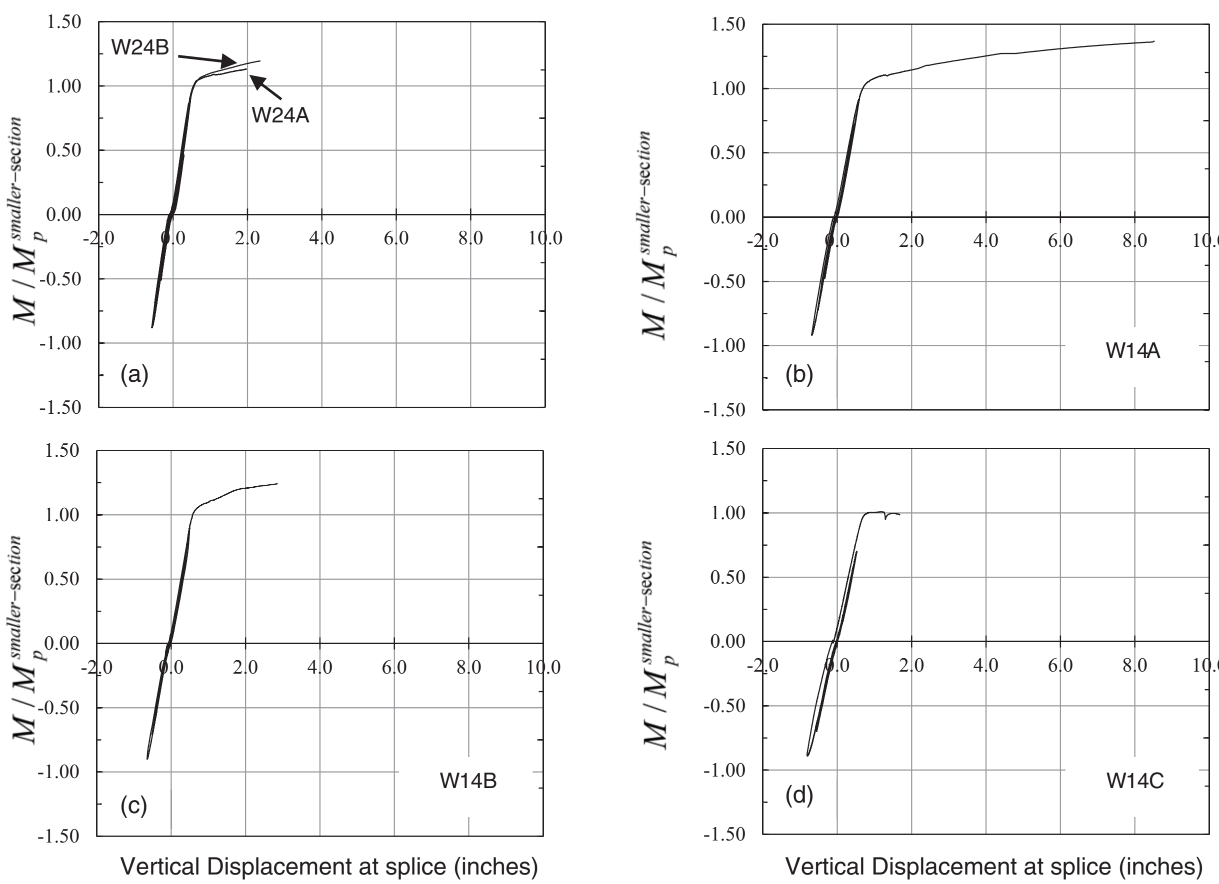


*Fig. 6. Load displacement curves for full-scale tests: (a) W24A and B; (b) W14A; (c) W14B; (d) W14C.*

summarized in Table 2. Other indicators of performance, such as the total deformation of the column provide a general, qualitative understanding of specimen response. The following discussion, which outlines the test data from each of these splices individually, is based on these results presented in Table 2 and Figure 6.

### *Response of Specimens 24A and 24B*

Referring to Figure 6a, both these specimens exhibited virtually identical response. The initial cycles produced no observable signs of distress. However, during the cycles with amplitude $0.95M_p$, minor flaking of the mill scale was observed in the vicinity of the splice, indicating the onset of yielding. During the final, monotonic push, widespread yielding was observed in the splice region, as well as the surrounding areas, including in both the smaller and the larger column sections. The test was concluded when fracture was suddenly observed at a force corresponding to the development of the splice moment $M_{splice} = 1.13 \times M_p^{smaller-section}$ for specimen 24A and $M_{splice} = 1.19 \times M_p^{smaller-section}$ for specimen 24B. The fracture initiated at the tip of the UWR and the surface was coincident with the heat-affected zone (HAZ). Based on an inverse section analysis (using the measured stress-strain data from the materials), weld stress, $\sigma_{flange}$, at the instant of fracture was estimated to be approximately $1.32F_y^{flange}$, where $F_y^{flange}$ is the measured yield stress of the particular section (Table 3). This suggests that the weld was fully yielded at the PJP section, and that the net section strength of this section was achieved. Also at this instant, the shear force in the splice, $V_{splice}$, was $0.85V_y^{smaller\text{-}section}$, where $V_y^{smaller\text{-}section} = 0.6F_y A_{web}^{smaller-section}$. The fracture completely severed the tension flange and propagated up through the PJP weld in the web, severing most of the web. Several bolts in the erection plate fractured as the crack propagated through the web weld. Figures 7a and 7b show photographs of both the tests taken after fracture.

### *Response of Specimen 14A*

Similar to specimens 24A and 24B, the initial loading cycles produced no observable signs of distress in the specimen. However, during the cycles with amplitude $0.95\boldsymbol{M_p}$, minor flaking of the mill scale was observed in the vicinity of the splice, indicating the onset of yielding. During the final push, large-scale yielding was observed in the splice, accompanied by widespread flaking of mill scale and the formation of visible slip bands. Figure 6b shows the load-deformation response, whereas Figure 7c shows a photograph of the specimen after the conclusion of the experiment. Referring to Figure 7c, fracture propagation was not observed for this experiment, which had to be concluded owing to safety concerns, wherein the applied load approached the capacity of the laboratory strong floor. Shown in Figure 7d is a closeup view of the unfused weld root. Small cracks (approximately 0.5 in. long) initiated at both tips. The degree of inelastic deformation in this specimen is striking. At the conclusion of the test, the estimated weld stresses, $\sigma_{flange}$, are approximately $1.34F_y^{flange}$. At this time, the moment in the splice, $M_{splice}$, was $1.37M_p^{smaller\text{-}splice}$, whereas the shear in the splice, $V_{splice}$, was equal to $0.93V_y^{smaller\text{-}section}$.

### *Response of Specimen 14B*

Similar to the other specimens, the initial loading cycles produced no observable signs of distress in the specimen. During the final push, large-scale yielding was observed in the splice, accompanied by widespread flaking of mill scale and the formation of visible slip bands. Figure 6c shows the load-deformation curve, while Figure 7e shows a photograph of the specimen after the conclusion of the experiment. Qualitatively, the response of the specimen was similar to that of specimen 14A, except that fracture was observed during the final push, when the moment in the splice, $M_{splice}$, was $1.24M_p^{smaller\text{-}splice}$, whereas shear in the splice, $V_{splice}$, was $0.86V_y^{smaller\text{-}section}$. The estimated weld stresses, $\sigma_{flange}$, (based on strain gage data) are approximately $1.34F_y^{flange}$.

### *Response of Specimen 14C*

Specimen 14C featured a bolted web plate, with no weld connection between the webs. Figures 6d and 7f show the load-deformation curve and post-test photograph, respectively. The response of this specimen was somewhat different than the other specimens, primarily in that yielding was observed at lower moments; in fact, some yielding was observed even in the cycles corresponding to $0.75M_p$. This may be attributed to the absence of full stress transfer through the web, in the tension region, such that development of full moment capacity is not theoretically possible. However, fracture was not observed until the final push—Figure 7f shows a post-test photograph. At the time of fracture, the moment in the splice, $M_{splice}$, was $1.04M_p^{smaller\text{-}section}$, whereas the shear in the splice, $V_{splice}$, was $0.72V_y^{smaller\text{-}section}$. Thus, even when judged relative to the entire loading protocol, the connection exhibited excellent performance. It is important to recall here that this detail, with the bolted web splice (and associated section sizes) is targeted toward low-rise structures, where the demands are quite low—refer, for example, to Table 1. When evaluated in this context, the response of the specimen is even more impressive. The strain rosette attached to the web splice plate recorded negligible shear strain. When combined with the observation that negligible shear deformation was noted in the flanges, this suggests that the shear was predominantly transferred through friction in the bearing portion of the sections, which provides the most rigid load path for the shear. This bearing zone develops as a result of the flexure in the cross-section. Two points may be made based on this observation. First, adequate friction was likely generated even in the absence of net axial compression, which is typically present in low-rise buildings, wherein overturning moments are low. Second, unlike moment connections, in which the shear tab separates the web of the beam from the flange of the column, friction may be a reliable mechanism of shear transfer in column splices where the sections are in direct contact. In summary, it appears that other than the loss of some flexural capacity (due to the unavailability of the web in the tension region), the absence of a welded web splice does not compromise the effectiveness of the connection in any significant way.

## Analysis and Discussion

The preceding sections provide specific discussion of individual specimen response. Based on this discussion, several general observations are now presented to evaluate the

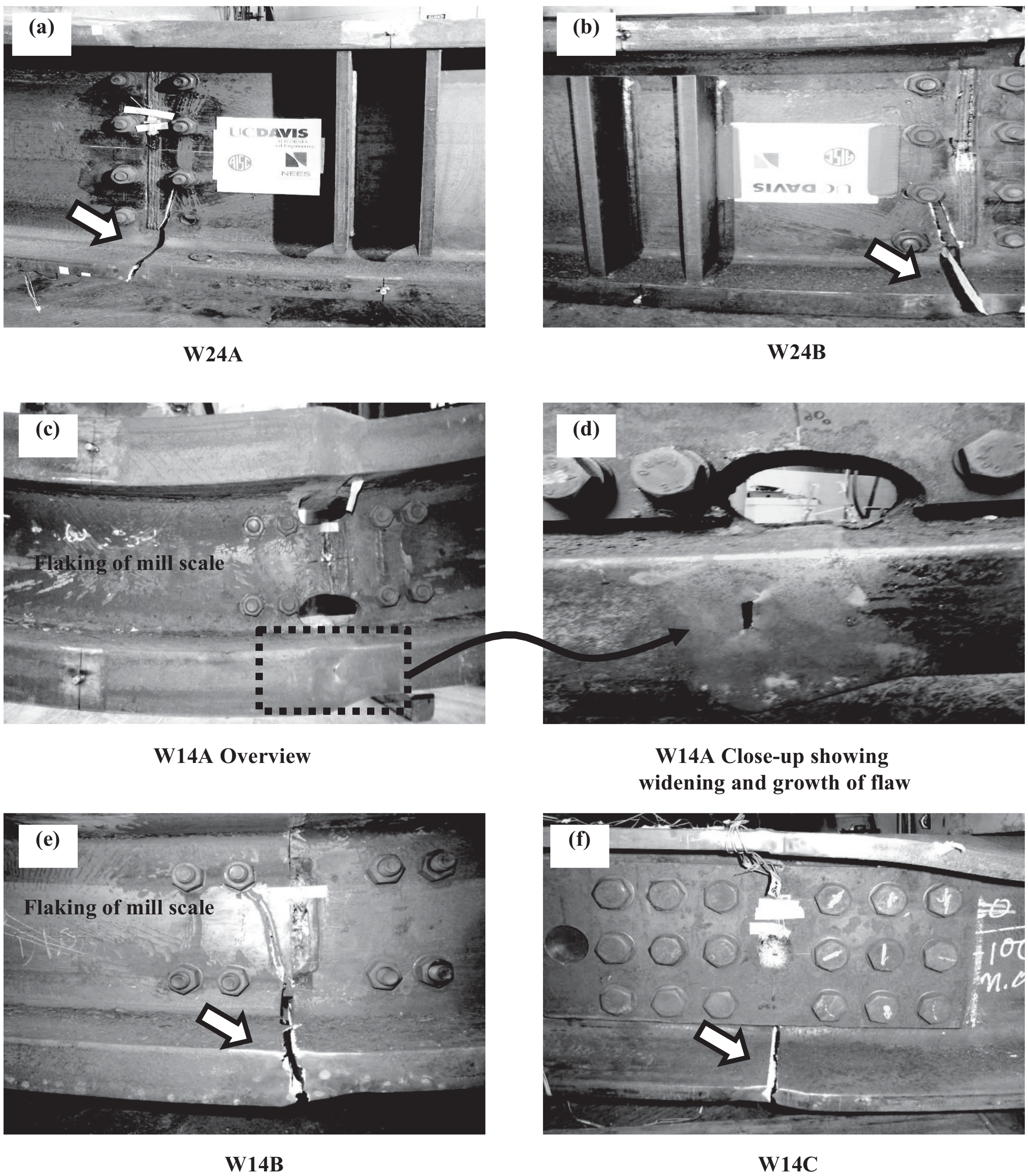


*Fig. 7. Post-test photographs of all the specimens; block arrows indicate fracture.*

suitability of these types of connections in IMRF and SMRF structures in highly seismic regions. The main observations are:

1. All specimens survived the cyclic portion of the protocol, and all (with the exception of specimen 14A) fractured on the final push. Recall that the protocol (if applied through completion) represents peak expected demands in 20-story buildings subjected to 2/50 ground motions. In this context, all the specimens (as tested in the lab) may be considered suitable candidates for application in such buildings.

2. In addition to exceeding the demands implied by the protocol, all the specimens also show significant inelastic deformation capacity. Referring to Table 2, the displacements (recorded at the midspan of the specimen) were several times yield displacement. Referring to previous discussion on demands, recall that column splices are mainly force-controlled components, with little expectation of inelastic action.

3. All the splice specimens were subjected to intense shear at the time of fracture. The shear demands in these splices were in the range of $0.72V_y^{smaller\text{-}section}$ to $0.93V_y^{smaller\text{-}section}$. This is significantly higher than may be expected in archetype buildings, wherein high moments at the splice location (which is typically near the center of the column) are accompanied by low shear because this type of response is associated with single curvature bending of the column associated with higher mode response. Recall that the test setup utilized by Bruneau and Mahin (1991) did not apply shear to the splices.

4. Two of the specimens featured somewhat innovative details: specimen 14B did not have a weld access hole, despite the presence of a weld on the inside of the web; and specimen 14C did not feature a welded web splice. Both these details exhibited excellent performance.

These observations indicate that the as-tested details are suitable for resisting seismic demands in moment frames. However, additional analysis needs to be conducted to generalize the test results to evaluate the possibility of their implementation in field details. For example, while the observed performance exceeded anticipated demands, the material toughness properties (specifically the weld properties, see Table 3) also exceeded the minimum required. Thus, extrapolation of the test results to field details (for which only minimum toughness may be relied upon, but which also will have reduced demands relative to the test splices) cannot be conducted without fracture mechanics analysis. The next section presents such an analysis.

## FRACTURE MECHANICS ANALYSIS OF SPLICE CONNECTIONS

The primary purpose of the fracture mechanics simulations presented in this section is to provide support for generalization of the experimental findings. The following points define the scope and intent of the simulations—

1. The main objective of the simulations is to examine the fracture toughness demands (represented by a stress intensity factor $K_I$), and its relationship to applied stresses in the column flange. This relationship may be used to evaluate the suitability of current material toughness requirements for details similar to the ones tested in the study.

2. The simulations did not examine details distinct (in terms of shapes welded, extent of penetration or other features) from the ones tested in this study. This is because:

   a. In terms of configuration, it is anticipated that the test specimens represent key geometric aspects of PJP-welded splices, which may be considered for use in the future.

   b. The test splices are fairly large, and fracture mechanics results based on larger specimens are in general conservative when applied to geometrically similar details that are smaller (Anderson, 1995; Bažant, 1984). Thus while not precise, a simulation of the test specimens provides a reasonable basis for extrapolation to similar details that are physically smaller in size

   c. A full parametric study examining all possible types of splice details and sizes is prohibitively expensive.

Fracture mechanics simulations were conducted for the flange regions of four specimens: W14A, W24A and B (identical simulation, given that the specimens are nominally identical) and W14C. The specimen W14B was not simulated, because the termination of the internal weld would require 3D simulation. All simulations were conducted using the commercial platform ABAQUS (ABAQUS, 2012). Figure 8 schematically illustrates a finite element mesh for one such simulation (shown for the W24 specimen); the mesh for the W14C specimen is qualitatively similar. The mesh for W14A is somewhat different to accommodate the embedded crack with two crack tips (refer Shaw, 2013). Key features of the simulations are:

1. All the simulations modeled only the flange region of the splices, subjected to pure tension. This is based on the assumption that this loading state controls the fracture toughness demands at the UWR. As shown

in Figure 8, the models were 2D plane-strain models, because stress variations through the width of the flange are relatively modest and the plane strain approximation represents out of plane constraint in a conservative manner. This modeling approach has been previously adopted with good agreement with test data by Nuttayasakul (2000).

2. Each simulation featured approximately 20,000 plane-strain 8-node quadrilateral elements, although 114,000 were used for the W14A simulation due to the two crack tips. As indicated in the inset in Figure 8, the crack tip was greatly refined at the tip of the flaw, such that the smallest element size was on the order of 0.0005 in. The crack tip was modeled with a diameter of 0.001 in. (significantly lower than the anticipated critical crack tip opening displacement, *CTOD*c, for structural steels, which is typically on the order of 0.01 in.). This type of finite element mesh at the crack tip has been shown to adequately capture the stress gradients as well as the effects of crack tip blunting through the work of McMeeking and Parks (1979) and subsequently Kanvinde and Deierlein (2006).

3. Material constitutive properties were based on von Mises plasticity with isotropic hardening. For the base material, the properties were calibrated from the coupon tests described previously and summarized in Table 3. For the weld material, all-weld coupon data (for a similar type of weld) generated previously by Kanvinde et al. (2008) was used for calibration.

4. Loading was applied in the form of a stress traction on the smaller (top) flange as shown in Figure 8. The contour J-integral (Rice, 1968) was evaluated at each loading step. The J-integral is a well-established index for characterizing fracture toughness demands (and capacities) in steel component with small to moderate yielding. The ABAQUS platform provides functionality for calculation of the J-integral. For each loading step, the J-integral was calculated from approximately 40 contours around the crack tip to minimize numerical inconsistencies. The J-integral ($J_I$, where the subscript $I$ denotes mode I, or crack opening) may be converted to an equivalent stress intensity factor $K_I$ (which may be interpreted as toughness demand) as per the following relationship:

$$K_I = \sqrt{EJ_I/\left(1-\nu^2\right)} \tag{1}$$

where $E$ is the elastic modulus, ksi, and ν is Poisson's ratio.

Figures 9a, 9b and 9c illustrate the results of the W24, W14A and W14C simulations, respectively. To interpret these figures effectively, it is useful to consider relationships between the CVN energy (for which minimum values are required as per AISC 341-10) and the critical stress intensity factor $K_{IC}$ (which is a measure of the fracture toughness capacity). One such relationship (based on statistical correlation) is provided by Barsom and Rolfe (1999). Equation 2 illustrates this relationship:

$$K_{IC}^{dynamic} = 0.001\sqrt{5000 \times CVN \times E} \tag{2}$$

In the previous equation *CVN* is the Charpy energy in ft-lb, $E$ is the modulus of elasticity in ksi, and $K_{IC}^{dynamic}$ is the stress intensity factor (in ksi$\sqrt{\text{in.}}$ under dynamic loading rates (because it is derived from the CVN data which is obtained from high-rate dynamic tests). In contrast, loading rates in the tests described in this paper, or even in field

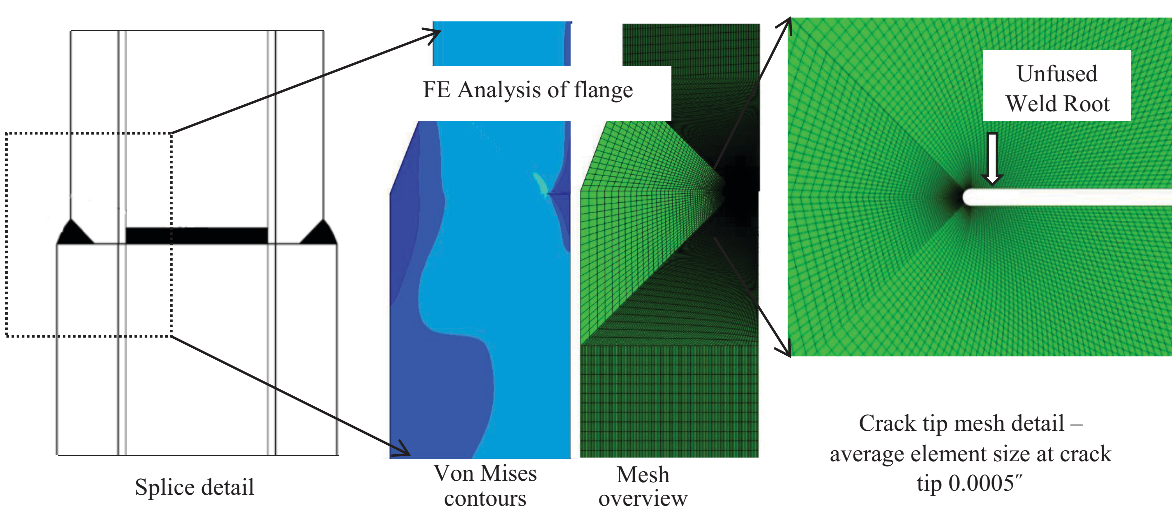


*Fig. 8. Finite element simulation of splice flanges (W24 simulation shown as representative).*

details subjected to earthquakes, may be considered "static," because they are several orders of magnitude lower than those observed in CVN tests (Barsom and Rolfe, 1999). In general, the $K_{IC}^{dynamic}$ is a lower bound on the available fracture toughness in seismic details. In each of the figures, the stress intensity factor $K_I$ determined from the finite element simulations is plotted against the applied stress in the smaller flange. Because W14A has two crack tips, Figure 9b has two curves. However, these are almost coincident indicating that the fracture toughness demand at both crack tips is virtually identical.

A close inspection of Figures 9a through 9c provides the following insights:

1. For all the simulations, the $K_I$ increases, as expected, monotonically with respect to the applied stress level. The points labeled *test performance* on the figures indicate the estimated longitudinal stress in the flange in each of the specimens at the time of fracture (based on an inverse sectional analysis outlined earlier). Referring to these labels on the figure, these stresses are in 65- to 75-ksi range. At these stresses, $K_I$ is in the range of 150 to 200 ksi$\sqrt{\text{in.}}$, implying it to be the available fracture toughness at the crack tips in the full-scale specimens. For comparison, if the CVN values from the PQR assembly (52 ft-lb) or the post-test weld from the W14B specimen (50 ft-lb) are converted to equivalent $K_{IC}^{dynamic}$ values per Equation 2, then $K_{IC}^{dynamic} \approx 85$ ksi$\sqrt{\text{in.}}$ The difference—the significantly higher implied toughness in the splice simulations as compared to $K_{IC}^{dynamic} \approx 85$ ksi$\sqrt{\text{in.}}$ determined previously—is not entirely surprising because both of the PQR tests as well as the W14B CVN tests are dynamic, such that 85 ksi$\sqrt{\text{in.}}$ is a lower bound on the available toughness; and the PQR tests were conducted at a lower temperature (0 °F), which is lower than the temperature at which the full-scale tests (approximately 60 °F) were conducted. In fact, the value $K_I \approx 150$ to 200 ksi$\sqrt{\text{in.}}$ is in the range of fracture toughness values for similar weld materials tested using static (rather than dynamic) fracture mechanics tests (Kanvinde et al., 2008).

2. In each of the Figures 9a through 9c, the marker *peak demands* indicates the maximum anticipated stress in the splice flange based on the nonlinear time history simulations described earlier. This is equal to the expected yield stress, approximately 55 ksi. Based on the intersection of this marker with the curves in Figures 9a through 9c, the toughness demands at this value of flange stress are 45 ksi$\sqrt{\text{in.}}$, 26 ksi$\sqrt{\text{in.}}$ and 27 ksi$\sqrt{\text{in.}}$ for W24, W14A and W14C, respectively. Also shown in the figures is the horizontal line labeled *minimum expected toughness*. This value, *K*IC = 54 ksi$\sqrt{\text{in.}}$, is obtained by substituting CVN = 20 ft-lb into Equation 2. The value of 20 ft-lb may be considered a suitable lower bound for material toughness because, for the weld filler metal, a value of 20 ft-lb at 0 °F is required; and for heavy sections (base metal), a CVN value 20 ft-lb at 70 °F in the core of the section is required; toughness elsewhere will likely be higher. As a result, $K_{IC} = 54$ ksi$\sqrt{\text{in.}}$ is a reasonable lower bound on the expected toughness in a demand critical weld, such as the PJP welds in splices. Relative to this value, the demands are lower (see Figure 9), suggesting that the splice details tested in this study are suitable for field use even if a low estimate of material toughness is considered. A possible exception to this is in the case of buildings where the column splices may be exposed to low temperatures (50 °F and lower), because the base metal toughness requirement (20 ft-lb) is applicable at 70 °F. AISC 341-10 requires that "the minimum qualification temperature for AWS D1.8/D1.8M Annex A be adjusted such that the test

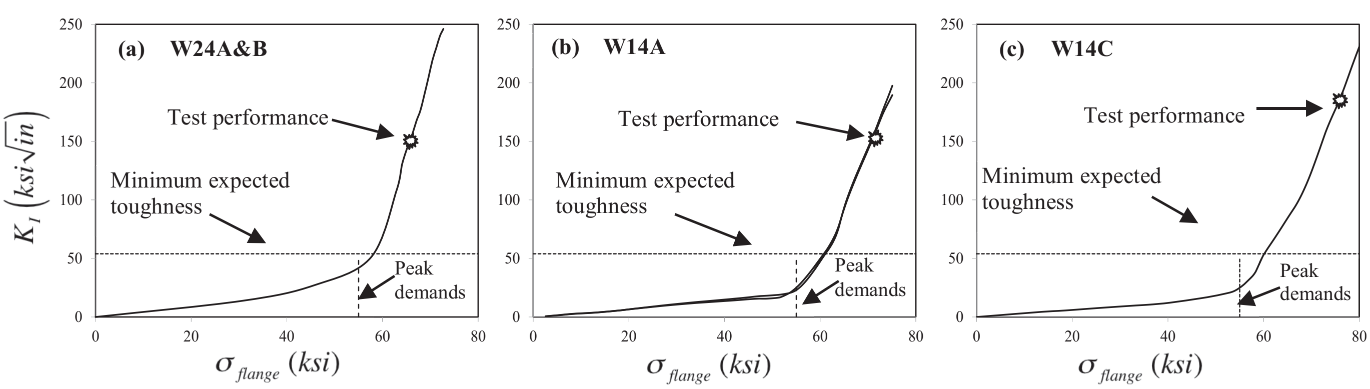


*Fig. 9. Results of finite element simulations for (a) W24 specimens; (b) W14A; and (c) W14C.*

temperature for the Charpy V-notch toughness qualification tests be no more than 20 °F (11 °C) above the lowest anticipated service temperature (LAST)."

In summary, the finite element simulations provide quantitative insight into the relationships between fracture toughness demands and applied stresses. For the connection details tested in this study, it is apparent that the toughness demands are lower as compared to the minimum available toughness capacity. This provides a suitable basis for generalizing the test results to connections that are geometrically similar to (and smaller than) the ones tested in this study. The next section summarizes the study along with its findings, implications, and limitations.

## SUMMARY AND CONCLUSIONS

AISC 341-10 requires the use of complete-joint-penetration (CJP) groove welds for column splices in intermediate and special moment frames in seismic design. These requirements are a result of research following the Northridge Earthquake on welded beam-column connections (SAC, 1996) that demonstrated the detrimental effect of embedded flaws (such as those produced at PJP welds) on the response of welded joints. However, more recent research (Myers et al., 2009; Gomez et al., 2010; and Dubina and Stratan, 2002) indicates that when high-toughness materials are used (as also mandated by post-Northridge design standards), then excellent performance may be obtained even if a flaw is present. Motivated by this research, the main objective of the current study is to examine the feasibility of PJP-welded column splices for steel moment frame construction in seismic regions.

The main scientific component of this study is a series of five full-scale column splice tests. The full-scale tests are supported by a comprehensive program of nonlinear time history simulation as well as ancillary material tests. The objective of the simulations is to quantitatively establish force and moment demands in the splices, ultimately leading to the development of a loading protocol for the full-scale experiments. The ancillary tests enable the interpretation of full-scale test data with respect to measured, rather than specified, material properties. The program of testing is also complemented by finite element simulations that employ fracture mechanics to develop support for the generalization of test results.

The full-scale test matrix includes a range of column sizes and details. The key variables interrogated in the test matrix include:

1. Column size, such that the tested specimens included sections from W14×132 to W14×730 with approximately 5-in.-thick flanges, as well as two specimens featuring W24 sections. The sizes represent commonly used sections for 4- to 20-story buildings.
2. Weld details, including single-bevel (W14C, W24A and B), and double-bevel specimens with (W14A) and without (W14B) a weld-access hole.
3. The absence of a welded web on one of the specimens (W14C) to examine the feasibility of bolted web connections for low-rise construction where the demands are modest.

The specimens were all subjected to reversed cyclic loading as per a loading protocol based on the nonlinear time history simulations. The load was applied in a three-point bend configuration such that the splice was subjected to a combination of flexure and shear. All the specimens exhibited excellent performance, surviving the entire loading protocol. Four out of the five specimens fractured in the tension flange of the splice during the final monotonic push after completion of the protocol. One specimen, W14A, did not fracture before machine capacity was reached, requiring the termination of the test. All specimens showed a high degree of inelastic deformation prior to fracture with yielding in both the larger and smaller column. Given that inelastic action is not expected in column splices (based on design intent as well as simulation), this performance is especially impressive. The peak moment sustained by the splices was in the range of $1.04M_p^{smaller\text{-}section}$ for the bolted web, and the W14C specimen was $1.37M_p^{smaller\text{-}section}$ for the W14A specimen, indicating that these splices developed the strength of the smaller connected column. The shear in these splices ranged from $0.72V_y^{smaller\text{-}section}$ to $0.93V_y^{smaller\text{-}section}$; these combinations of high moment and shear are highly unlikely in an archetype frame.

A series of fracture mechanics simulations was conducted to develop support for the generalization of test results. The main objective of the finite element simulations was to examine the relationship between the fracture toughness demand (represented by the stress intensity factor $K_I$, and the applied stress in the flange). The simulations indicated that for the tested connections, the toughness demands are below the minimum expected toughness (considering the requirements of AISC 341-10). This suggests that details similar to the ones tested in the study may be suitable for general use in the field. While the results of the study are encouraging from the perspective of adoption of PJP splices in IMRFs and SMRFs, the study has several limitations that must be considered when interpreting the results:

1. While the experiments incorporated a range of details and member sizes, field details that are significantly dissimilar to the tested specimens may have higher toughness demands, and thus be more fracture critical. Examples of these situations include details where the extent of weld penetration or effective throat thickness is smaller (and the UWR is larger) than in the tests and details where flanges of similar thickness

are connected, where the reinforcement provided by the flared shape of the weld is absent (in contrast to the unequal flange connection where significant reinforcement is present due to the shape of the weld transition; see Figure 5). An accurate assessment of these factors is possible only through additional testing or a comprehensive parametric study using finite element simulations similar to the ones described in this paper.

2. A rigorous reliability analysis to determine capacity factors ($\phi$ factors) for design of these connections has not been conducted, neither has a strength characterization approach been developed. These are subjects of ongoing study. However, based on the performance of these details, and the insights provided by the finite element simulations, a possible route for implementation of this research is the prescriptive use of details similar to the ones tested.

3. The toughness estimate used in the fracture mechanics analysis (20 ft-lb) may not be conservative for columns that are exposed to low temperatures (50 °F and lower), because the base metal (in the core of heavy sections) toughness is required at 70 °F. AISC 341-10 requires that toughness qualification tests be no more than 20 °F above the lowest anticipated service temperature. It is also pertinent to mention here that the 20 ft-lb at 70 °F toughness (in the core) is not required when the column flanges are thinner than 1½ in., because adequate toughness is expected from these. Consequently, while it is highly likely that the results of this study are applicable to these situations (test 14C supports this), it is noted that the 20 ft-lb toughness is not explicitly required by the AISC 341-10 for these situations.

4. Residual stresses in welds, as well as in-situ weld toughness are sensitive to parameters of the welding procedures as well as physical constraints at the time of welding (Masubuchi, 1980). This should be considered as a factor in the generalization/implementation of results.

5. The demand analysis (the nonlinear time history simulations) is based on a small set of archetype buildings subjected to a limited number of ground motions. While the results of this analysis are applied in a conservative manner, aspects of structural response not considered by the simulation (e.g., buildings taller than 20 stories, near fault ground motions and vertical accelerations) may influence demands in the splices. Similarly, the effect of the use of high-strength steel for columns on splice demands is also undetermined. As discussed previously, columns with Grade 50 material ($F_y = 50$ ksi) were used along with E70 welds. However, given that the columns in the nonlinear time history simulations showed very limited (or no) yielding, it may be argued that the strength of the columns may not affect demands in the splices.

6. Because the nonlinear time history simulations are based on planar frames, three-dimensional effects (due to bidirectional shaking) are not explicitly incorporated in this study. However, the effects of this are anticipated to be modest. Moreover, it is important to recall that the simulations only featured special moment resisting frames and not intermediate moment frames (IMFs), which are not subject to the SCWB requirement. Thus, it may be argued that the results are not applicable to IMFs wherein the splice force/moment demands may be larger. However, two points may be made in response. First, even in the SMRFs (considered in this study), which have the SCWB requirement, the column end interaction ratio approached yield for the 20-story frame. Second, IMFs are limited to a 35-ft height restriction in seismic design category D. The nonlinear time history results for the 4-story SMRF (which is similar in height to this limit) suggest that the response in these cases is dominated by first mode response with low demands at the splice. It is not unrealistic to extrapolate this response to IMFs.

7. While the effects of these factors have not been determined, in some ways, the results of the study may also be conservative with respect to field conditions. For example, the test specimens required flipping for the application of reversed cyclic loading. Each of these flips required approximately 1 to 2 hr to execute, introducing the possibility of strain aging and associated detrimental effects on splice performance. These effects are not present in field splices, which are subject to a higher rate of loading.

Thus, while the results of this study are promising from a standpoint of utilizing PJP-welded splices in seismic moment frames, some of the issues previously discussed need to be considered in adopting these findings in standards. While it may not be feasible to conduct additional full-scale testing, focused parametric simulation through FE simulation may greatly aid the generalization and implementation of these results.

## ACKNOWLEDGMENTS

This project was funded by the American Institute of Steel Construction (AISC). Herrick Steel of Stockton, California, and Gayle Manufacturing Company of Woodland, California, generously donated and fabricated steel materials for this research, and their donations are gratefully acknowledged.

California Erectors of Benicia, California, donated its time toward welding of the specimens. The authors also thank Tom Schlafly of AISC, Bob Hazelton of Herrick Steel, and Gary Glenn of Gayle Manufacturing in addition to the AISC research committee, specifically James Malley and John Barsom, for providing oversight and direction to the testing plans and interpretation of results. The large-scale experiments described in this report were conducted at the Network for Earthquake Engineering Simulation (NEES) equipment site at the University of California at Berkeley in Richmond, California. The authors would also acknowledge the NEES and William Vuong, undergraduate researcher from the University of California at Davis, for assisting with the testing. The findings and opinions of this paper are those of the authors and do not necessarily represent those of the major sponsor, AISC.

## SYMBOLS

$CTOD_c$ Critical crack tip opening displacement.

$E$ Modulus of elasticity of steel, 29,000 ksi.

$F_y$ Specified yield stress.

$F_y^{flange}$ Measured yield stress of smaller column flange.

$IR$ Interaction ratio of column section, defined as

$$IR = \frac{P}{P_y} + \frac{8}{9}\frac{M}{M_p} \text{ for } \frac{P}{P_y} \geq 0.2$$

$$IR = \frac{P}{2P_y} + \frac{M}{M_p} \text{ for } \frac{P}{P_y} < 0.2$$

where $P_y$ and $M_p$ are the axial force capacity and plastic moment capacities, respectively, of the smaller column. $P$ and $M$ are force and moment, respectively, at the splice.

$IR_{peak}^{median}$, $IR_{peak}^{\max}$ The median and maximum (over 20 ground motions) values of the peak interaction ratio (peak within each time history).

$J_I$ J-integral for mode I.

$K_I$, $K_{IC}$ Stress intensity factor demand, capacity.

$M_{splice}$ Applied moment at the splice.

$M_p^{smaller-section}$ Plastic moment capacity of the smaller cross section such that $M_p^{smaller-section} = R_y F_y Z_x$, where $R_y$ is the ratio of the estimated to specified yield strength, and $Z_x$ is the plastic section modulus of the smaller section.

$M_{splice}^{\max}$ Maximum moment observed in the splice during experiment.

$V_{splice}^{\max}$ Maximum shear observed in the splice during experiment.

$V_y^{smaller\text{-}section}$ Shear strength of the smaller cross-section, equal to $0.6F_y A_{web}^{smaller-section}$.

$\Delta_{peak}^{median}$, $\Delta_{peak}^{\max}$ The median and maximum (over 20 ground motions) values of the peak interstory drift (peak within each time history).

$\nu$ Poisson's ratio, 0.3.

$\sigma_{flange}$ Estimated stress in the tension flange based on section analysis.

## REFERENCES

ABAQUS (2012), *User's Manual*, Hibbitt, Karlsson, and Sorensen, Inc., Providence, RI.

AISC (2010), *Seismic Provisions for Structural Steel Buildings*, AISC 341-10, American Institute of Steel Construction, Chicago, IL.

AISC (2011), *Steel Construction Manual*, 14th Ed., American Institute of Steel Construction, Chicago, IL.

Anderson, T.L. (1995), *Fracture Mechanics*, 2nd Ed., CRC Press, Boca Raton, FL.

ASCE (2010), *Minimum Design Loads for Buildings and Other Structures*, ASCE 7, American Society of Civil Engineers, Reston, VA.

AWS (2004), *Structural Welding Code—Steel,* AWS D1.1/D1.1M: 2004, American Welding Society, Miami, FL.

AWS (2009), *Structural Welding Code—Seismic Supplement*, AWS D1.8/D1.8M: 2009, American Welding Society, Miami, FL.

Barsom, J.M. and Rolfe, S.T. (1999), *Fracture and Fatigue Control in Structures*, 3rd ed., Butterworth-Heinemann, Waltham, MA.

Bažant, Z.P. (1984), "Size Effect in Blunt Fracture: Concrete, Rock, Metal," *Journal of Engineering Mechanics,* ASCE, Vol. 110, No. 4, pp. 518–535.

Bruneau, M. and Mahin, S., (1991), "Full-scale tests of Butt-Welded Splices in Heavy-Rolled Steel Sections Subjected to Primary Tensile Stresses," *Engineering Journal*, AISC, First Quarter, pp. 1–17.

Dubina, D. and Stratan, A. (2002), "Behaviour of Welded Connections of Moment Resisting Frames Beam-to-Column Joints," *Engineering Structures,* Elsevier, Vol. 24, No. 11, pp. 1431–1440.

Engelhardt, M.D. and Sabol, T.A. (1994), "Testing of Welded Steel Moment Connections in Response to the Northridge Earthquake," Research Progress Report, Northridge Steel Update I, American Institute of Steel Construction, Chicago, IL.

Fell, B.V., Kanvinde, A.M., Deierlein, G.G. and Myers, A.T. (2009), "Experimental Investigation of Inelastic Cyclic Buckling and Fracture of Steel Braces," *Journal of Structural Engineering,* ASCE, Vol. 135, No. 1, pp. 19–32.

FEMA (2000), *Recommended Design Criteria for New Steel Moment-Frame Building*s, FEMA 350, Federal Emergency Management Agency, Washington, DC.

Gomez, I.R., Kanvinde, A.M. and Deierlein, G.G. (2010), "Exposed Column Base Connections Subjected to Axial Compression and Flexure," Report Submitted to the American Institute of Steel Construction, Chicago, IL.

Gupta, A. and Krawinkler, H. (1999), "Seismic Demands for Performance Evaluation of Steel Moment Resisting Frame Structures, (SAC Task 5.4.3), Report No. 132, John A. Blume Earthquake Engineering Center, Stanford University, Stanford, CA.

Hayes, J.M. (1957), "Effects of Initial Eccentricities on Column Performance and Capacity," *Journal of the Structural Division*, American Society of Civil Engineers, Paper 1440.

Kanvinde A.M. and Deierlein G.G. (2006), "The Void Growth Model and the Stress Modified Critical Strain Model to Predict Ductile Fracture in Structural Steels" *Journal of Structural Engineering,* ASCE, Vol. 132, No. 12, pp. 1907–1918.

Kanvinde A.M., Fell B.V., Gomez I.R. and Roberts M. (2008), "Predicting Fracture in Structural Fillet Welds Using Traditional and Micromechanics-Based Models," *Engineering Structures,* Elsevier, Vol. 30, No. 11, pp. 3325–3335.

Kaufman, E. and Fisher, J. (1995), "A Study of the Effects of Materials and Welding Factors on Moment Frame Weld Joint Performance Using a Small-scale Tension Specimen," *Technical Report 95-08*, SAC Joint Venture, Sacramento, CA, December.

Kaufmann, E.J., Metrovich, B.R., and Pense, A.W. (2001), "Characterization of Cyclic Inelastic Strain Behavior on Properties of A572 Gr. 50 and A913 Gr. 50 Rolled Sections," Final Report to American Institute of Steel Construction, ATLSS Report 01-13, Lehigh University, Bethlehem, PA.

Lignos, D.G., Krawinkler, H. and Whittaker, A. S. (2011), "Prediction and Validation of Sidesway Collapse of Two Scale Models of a 4-Story Steel Moment Frame," *Earthquake Engineering and Structural Dynamics,* Vol. 40, No. 7, pp. 807–825.

Masubuchi, K., (1980), *Analysis of Welded Structures*, Pergamon Press, Elmsford, NY.

Matsuishi, M. and Endo, T. (1968), *Fatigue of Metals Subjected to Varying Stress*, Japan Society of Mechanical Engineering, Tokyo, Japan.

McMeeking, R.M. and Parks, D.M. (1979), "On Criteria for J-Dominance of Crack-Tip Fields in Large Scale Yielding," *Elastic-Plastic Fracture*, ASTM STP 668, J.D. Landes, J.A. Begley and G.A. Clarke, Eds., American Society for Testing and Materials, West Conshohocken, PA, pp. 175–194.

Myers, A.T., Kanvinde, A.M., Deierlein, G.G. and Fell, B.V. (2009), "Effect of Weld Details on the Ductility of Steel Column Baseplate Connections," *Journal of Constructional Steel Research*, Elsevier, Vol. 65, No. 6, pp. 1366–1373.

Nuttaysakul, N. (2000), "Finite Element Fracture Mechanics Study of Partial Penetration Welded Splices," Master's Thesis, Stanford University, Stanford, CA.

OpenSEES (2009), "Open System for Earthquake Engineering Simulation," Pacific Earthquake Engineering Center, Berkeley, CA.

Popov, E.P. and Stephen, R.M. (1976), "Capacity of Columns with Splice Imperfections," *Engineering Journal,* American Institute of Steel Construction, First Quarter, pp. 16–23.

Rice, J.R. (1968), "A Path-Independent Integral and the Approximate Analysis of Strain Concentration for Notches and Cracks." *Journal of Applied Mechanics*, Vol. 35, pp. 379–386.

Richards, P.W. and Uang, C-M. (2006), "Testing Protocol for Short Links in Eccentrically Braced Frames," *Journal of Structural Engineering*, ASCE, Vol. 132, No. 8, pp. 1183–1191.

SAC Joint Venture (1996), "Selected Results from the SAC Phase 1 Beam-Column Connection Pre-Test Analyses," Technical Report 96-01, Sacramento, CA.

Shen, J, Sabol, T., Akabas, B. and Sutchiewcharn, C. (2010), "Seismic Demand of Column Splices in Special Moment Frames," *Engineering Journal,* AISC, Fourth Quarter, pp. 223–240.

Shaw, S.M., (2013), "Seismic Performance of Partial Joint Penetration Welds in Special Moment Resisting Frames," Ph.D. Dissertation, University of California, Davis, CA.

Somerville, P., Smith, N., Punyamurthula, S. and Sun, J. (1997), "Development of Ground Motion Time Histories for Phase 2 of the FEMA/SAC Steel Project," SAC Background Document, Report No. SAC/BD-97/04.